Viscoelasticity and Plasticity Considerations in the Fracture of Glasslike High Polymers [1]

L. C. Cessna, Jr.[2] and S. S. Sternstein

Department of Chemical Engineering
and
Materials Research Center
Rensselaer Polytechnic Institute
Troy, New York

September, 1966

GPO PRICE $ _____

CFSTI PRICE(S) $ _____

Hard copy (HC) 3.00

Microfiche (MF) .50

ff 653 July 65

FACILITY FORM 602

N66 39920 (ACCESSION NUMBER)

55 (PAGES)

CR 79113 (NASA CR OR TMX OR AD NUMBER)

(THRU) 1

(CODE) 18

(CATEGORY)

This paper was presented at a Symposium on Fracture sponsored by the Ilikon Corporation, Boston, Massachusetts, February, 1966. To be published in Fundamental Phenomena in the Material Sciences, Vol. 4 by Plenum Press, 1967.

---

(1) Paper presented by S. Sternstein.

(2) Present address: Hercules Research Center, Wilmington, Del.

Introduction

This paper is concerned with the fracture properties of amorphous, linear high polymers below the glass transition temperature and under conditions of loading such that material failure may be classified as apparently brittle. At extremely low rates of loading or at temperatures approaching the glass transition, the polymers of interest may also exhibit a ductile type of failure, and the relevance of the concepts presented to such a failure mode is also mentioned briefly.

It is well known that glasslike, linear high polymers are capable of inhomogeneous deformation processes. Craze formation is an example of such a non-uniform deformation system in which the stresses and deformations within the craze are markedly different from the corresponding quantities within the uncrazed "matrix," or bulk material. Since the formation of a craze represents an apparently plastic deformation, it follows that the size of the craze is not uniquely coupled to the load or deformation which acts at any instant on the bulk sample. Rather, the extent of apparently plastic deformation which constitutes the craze is coupled to the entire stress history of the flaw or defect which generated the stress concentration giving rise to a localized plastic deformation. Thus, it follows that knowledge of the initial stress concentration factor, the sample loading history, and the rheological response of the material to localized high stresses are required to define the path-dependent growth of a plastic region within an apparently glasslike matrix.

Attempts to apply the Griffith criterion (1), equation 1,

$$\sigma_B = \left[\frac{2E\gamma}{\pi c} \right]^{1/2} \qquad (1)$$

to tensile strength data of polystyrene (PS) and polymethylmethacrylate (PMMA) have indicated a number of conceptual difficulties. For example, it has been observed (2, 3) that PS and PMMA obey the Griffith equation qualitatively in that a plot of log σ_B versus log c, for artificial flaws of length c, gives a straight line of slope (-1/2). However, attempts to correlate the experimental values of γ_0, the Griffith surface energy, with theoretical estimates of γ indicate that the experimental value is generally two or three orders of magnitude larger than the value obtained by consideration of chain backbone bond strengths and densities (4). This "excess" value of γ has been attributed to the energy required to plastically deform and orient the macromolecules at the tip of a propagating crack in a glass-like high polymer (2, 3, 4).

Fracture surface morphology studies have shown conclusively that a high degree of localized deformation occurs near and on the surfaces formed by a propagating crack in a glasslike high polymer (5-10). However, a conceptual difficulty arises in attempting to extract information from the Griffith equation on plastic deformation which occurs during the actual propagation of a crack, since this equation is based on a criterion for crack instability, that is, the condition at which crack growth initiates.

While the presence of large scale deformation and orientation of material at the tip of a propagating crack cannot be denied, such deformations bear little direct relationship to the deformations at the crack tip which occur prior to crack propagation and which, of necessity, are dependent on the sample loading history. Thus, any plastic deformation at the tip of a stress concentrating flaw, prior to the onset of flaw instability, will be path-dependent and will result in a path-dependent modification, or alteration, of the stress concentration giving rise to the plastic deformation. Therefore, such plastic deformations do not constitute a material parameter, per se, but rather a path-dependent function of the sample loading history, initial stress concentration factor, rheological response of the

material, and the mutual interaction of the rheological response and stress concentration, all prior to failure.

Another conceptual difficulty in the application of the Griffith equation to glasslike high polymers is the observed decrease of γ with tensile test temperature (11), in contrast to the expected enhancement of plastic processes at elevated temperatures. Further limitations of the Griffith equation include its inability to account for time-dependent phenomena such as rate of loading effects on tensile strength or for creep failure, unless additional ad-hoc variations of γ are permitted.

A demonstration of the significance of plastic processes which occur prior to flaw instability, and which result in differences in observed tensile strength data, is shown in Figures 1 and 2. Samples of PMMA and PS which contained artificial flaws introduced at various temperatures were tensile tested at the same temperature and Figures 1 and 2 show the least-mean-squares lines obtained. Clearly, flaws of the same size exhibit varying degrees of stress concentrating ability which are dependent on the conditions of flaw introduction. The results of these experiments, which illustrate the non-unique applicability of the Griffith equation, have been interpreted in terms of the initial degree of plasticity which surrounds the flaw tip, as influenced by the flaw introduction temperature (12, 13). Thus, if the observed fracture strength is dependent on the conditions of flaw introduction as well as the conditions of the fracture test, then the Griffith surface energy cannot be considered a material parameter, as originally intended. The lack of a unique surface energy for high polymers has also been emphasized by Bikerman (17).

The effect of a zone of plastic deformation on the stress concentration factor of a crack has been considered (14, 15). Referring to Figure 3, if a crack of length c (or an ellipse of major axis 2c), oriented perpendicular to the axis of applied uniaxial stress, ends in a region of plastic deformation of extent $2\rho_o$,

measured in the direction shown, then the stress concentration factor is given by equation 2

$$Q_o = \frac{\hat{\sigma}}{\sigma} = 2A\sqrt{\frac{c}{\rho_o}} \qquad (2)$$

where Q_o is the stress concentration factor, σ is the applied stress, $\hat{\sigma}$ is the uniform stress in the plastic zone, A is a constant near unity, and c and ρ_o characterize the flaw as mentioned above. It is to be noted that the flaw tip, i.e., its radius of curvature, does not enter into equation 2 if a plastic zone surrounds the tip. However, in the absence of plasticity, the ρ_o of equation 2 becomes the radius of curvature of the flaw itself. Therefore, any plasticity or initiation of plasticity at the tip of a flaw can modify appreciably the stress concentrating ability of the flaw. For glasslike high polymers, consideration of such effects is essential to an understanding of the fracture process itself, as illustrated by Figures 1 and 2.

Incorporation of the plasticity modified stress concentration factor of equation 2 into a failure theory analogous to Griffith's theory results in equation 3, as obtained by Orowan (16):

$$\sigma_B = \frac{1}{2}\sqrt{\frac{2E\gamma\rho_B}{bc}} \qquad (3)$$

where ρ_B is the size of the plastic zone at the instant of failure, i.e., at the onset of crack propagation, and b is a molecular spacing constant. It is to be noted that if plasticity effects become negligible, then setting ρ_B equal to b gives the Orowan result for a sharp crack in an elastic medium, which is identical, within a constant, to the Griffith equation.

Using data (4) on the failure strengths of PMMA and PS and theoretical estimates of γ of the order of 500 ergs/cm^2, it is found from equation 3 that ρ_B is of the order of 1,000Å, which is in reasonable agreement with estimates of the depths of the oriented layers on the fracture surfaces of glassy polymers (8). Thus, using

the Orowan modification, it would appear that the anomalous behavior of γ , the surface energy term, may be accounted for by the allowance of a plastic zone at the flaw tip which exists prior to flaw propagation. This conclusion is in agreement with the results of Figures 1 and 2.

In view of the reasonable nature of the value of ρ_0 obtained above, a theory will now be presented which treats the general, time-dependent stress concentration factor - rheological response problem. Since amorphous glasslike high polymers exhibit localized plastic deformations which are time-dependent and stress-sensitive, the plastic zone at the tip of a flaw will vary in size during the sample loading history. But the size of the plastic zone will influence the stress concentration causing plastic and viscoelastic effects. Thus, the growth of a plastic zone determines its own future ability for growth.

A simultaneous solution of the equation which gives the stress concentration as a function of plastic zone size and the equation which describes the rheological response of the material to localized high stress is required. This solution will be path-dependent on the sample loading history and parametrically dependent on the initial value of the stress concentration factor, i.e., the character of the flaw. Only after solution for the stress history in the plastic zone can a localized criterion of failure be used to deduce when sample failure will occur. Formulated in such a manner, localized failure can be described by a material constant which is independent of the sample loading history (e.g. creep or constant strain rate) and sample conditions (e.g. temperature). However, sample loading history and temperature will influence the rheological response of the plastic zone and thereby alter the stress path in that region.

It is emphasized that equation 3 is not the solution to the stated problem, since that equation is derived for a plastic zone of constant size and hence does not incorporate the path-dependent solution for the stress concentration factor as required for the stress-sensitive, viscoelastic - plastic response of a glasslike

high polymer. The simultaneous solution outlined above is presented below for arbitrary sample loading history and arbitrary sample rheology. Specific solutions for PMMA, for the specified loading histories of creep and constant strain rate, are then given and compared with experimental results.

A detailed development of the theory, and its applications to PMMA, may be found elsewhere (18, 19).

Theory

The Critical Zone

For purposes of illustration, consider a flaw in the form of an edge crack of length c (see Figure 3) or an elliptical crack of major axis 2 c, oriented perpendicular to the applied uniaxial tension. Let the tip of the crack end in a plastic zone of thickness $2\rho_o$ measured parallel to the applied stress. It is assumed that the flaw under consideration represents the critical sample flaw, that is, the flaw with the highest initial stress concentration factor (as defined by equation 2). The region at the flaw tip where plastic deformations initiate and/or grow is referred to as the critical zone and is the region where local failure will initiate.

Because of the viscoelastic-plastic response of a glasslike high polymer to localized high stresses, the plastic region at the flaw tip will, in general, undergo a time-dependent growth with a path determined by the stress history of the critical zone and by the applied sample stress history. Since the stress concentration factor is dependent on the size of the plastic zone, it follows that growth of the zone will alter the driving force, or stress, for later growth. Thus, simultaneous solution of the stress concentration equation with the rheological equation describing the stress-deformation-time response of the material in the critical zone is required to determine the stress history of the plastic zone.

It is to be emphasized that the plastic deformation process referred to represents those deformations which occur during the sample loading history prior to failure initiation, i.e., crack or flaw propagation, in contradistinction to those plastic processes which occur during crack propagation. The latter manifest themselves in the fracture surface morphology through the kinetics of crack propagation. Presumably, both plastic processes are governed by the sample's rheological response to localized high stresses, but only those plastic deformations which occur prior to failure initiation are of concern here.

The growth of the critical zone may be likened to the growth of a craze during its initial stages of thickening in the direction of applied stress. Given proper conditions of stress, time, and environment, it has been demonstrated (20, 21) that the critical zone will ultimately propagate in the direction perpendicular to applied stress and become a visible craze.

It is recognized that, for a high polymer below its glass transition temperature, there is no abrupt boundary between the highly oriented plastic material in the critical zone and the bulk material, but a continuous gradient of high deformation which decays outward from the flaw tip. For a material with a true local yield stress, the critical zone would be identical to that first considered by Neuber (14) and would result in a stress concentration factor given by equation 2.

In order to develop a first approximation to the time dependence of the stress concentration factor, as influenced by the growth of a plastic zone, it is assumed that a stress averaged truly plastic zone of uniform stress can be substituted for the apparently plastic zone of continuous stress gradient. Thus, in Figure 3, 2 represents the average initial size of the plastic zone at the tip of the critical flaw. The initial stress concentration factor, prior to any sample loading, is then given by equation 2.

The load imposed on the bulk sample is greatly magnified in the critical zone and results in growth of the plastic zone to some size $2\rho(t)$ at a time t measured from the commencement of the sample loading history. The growth of the plastic zone results in a change of the stress concentration factor, assumed to be given by equation 2, which at time t is:

$$Q(t) = \frac{\tau(t)}{\sigma(t)} = 2A\sqrt{\frac{c}{\rho(t)}} \qquad (4)$$

In order to obtain a solution for the stress concentration factor, equation 4, as a function of time, it is necessary to obtain the size of the plastic zone, $\rho(t)$

as a function of time. For convenience, define a nominal strain for the plastic zone, $\delta(t)$, as follows:

$$\delta(t) = \frac{\rho(t) - \rho_0}{\rho_0} \tag{5}$$

Thus, $\delta(0) = 0$ at the initiation of the sample loading history. Substitution of equation 5 into equation 4 gives the stress concentration factor as a function of nominal strain (or relative growth) of the critical zone:

$$Q(t) = \frac{\hat{\tau}(t)}{\sigma(t)} = Q_0\left[1+\delta(t)\right]^{-1/2} \tag{6}$$

where Q_0 is the Neuber constant defined by equation 2, and represents the initial value of the stress concentration factor, that is, prior to any sample loading history.

It is now necessary to describe the growth of the viscoelastic-plastic zone at the flaw tip under the influence of the time-dependent high stress in the critical zone, as defined by equation 6. To illustrate the procedure, consider one possible rheological equation for the critical zone in the following form:

$$H\tilde{\tau} = J\delta \tag{7a}$$

where H is a time-dependent differential operator given by

$$H = a_0 + a_1\frac{d}{dt} + a_2\frac{d^2}{dt^2} + a_3\frac{d^3}{dt^3} + \cdots \tag{7b}$$

$$H = \sum_{i=0}^{N} a_i \frac{d^i}{dt^i}$$

and J is given, similarly, by

$$J = \sum_{j=0}^{M} b_j \frac{d^j}{dt^j} \tag{7c}$$

and where the a_i and b_i are functions of time and stress level $\tilde{\tau}$, in general, or are constants for a linear material. Equation 7 is only intended as an example rheological statement of the critical zone response and may be of different form depending on the material under consideration.

For a critical zone rheological equation of the form of equation 7, one of several ways to proceed with the simultaneous solution of equations 7 and 6 is as follows: Equation 6 may be used to eliminate the stress $\tilde{\tau}$ and its derivatives from equation 7. For example, from equation 6 one obtains

$$\frac{d\tilde{\tau}}{dt} = \dot{\tilde{\tau}} = Q_0\left\{\frac{\dot{\sigma}(t)}{[1+\delta(t)]^{1/2}} - \frac{\sigma(t)\,\dot{\delta}(t)}{2[1+\delta(t)]^{3/2}}\right\} \tag{8}$$

where the large dot denotes derivation with respect to time. Equation 8 can now be used to replace $\dot{\tilde{\tau}}$ where it occurs in equation 7 by derivatives on δ and on σ, the latter being known for a prescribed, but arbitrary, sample loading history.

Thus, a systematic reduction of equation 7 may be achieved in which all functions of $\tilde{\tau}$ are replaced by functions of δ and σ, thereby obtaining a differential equation in δ which contains prescribed sample loading functions, $\sigma(t)$, known rheological constants and the parameter Q_o. Solution of the resultant differential equation yields $\delta(t)$ which, when combined with equation 6 gives $Q(t)$, the desired result.

The procedure just outlined accounts for the mutual interaction of the stress concentration causing viscoelastic-plastic response of the critical zone, and the effect of the plastic response on the value of the stress concentration. In general, the method of solution outlined will yield different stress concentration paths $Q(t)$ depending on the chosen sample loading path $\sigma(t)$, the Neuber constant Q_o, and the particular rheological constants and equation for the given material. The procedure presented can, in principle, be applied to a material capable of any arbitrary localized viscoelastic-plastic response, which may or may not be describable by a rheological model of the form of equation 7.

The formulation of the critical zone concept presented here embodies the following four assumptions: (a) the deformation of the critical zone is essentially an isothermal process; (b) the applied sample stress history is uniaxial; (c) the stress concentration factor for the flaw tip may be obtained, to a first approximation, by a one-dimensional, but unsteady state and path-dependent, stress analysis of a plastic zone of uniform stress $\tilde{\tau}$ which grows at the flaw tip; (d) the growth of the plastic zone is essentially a constant mass process.

The first assumption limits the application of the theory to relatively low speed failure tests, and excludes application to dynamic conditions. However, low

frequency cyclical tests are probably included in this treatment. Some preliminary work on the problem of the adiabatic growth of the critical zone can be found elsewhere (18).

Limitations on the applications of this theory imposed by assumption "b" can be removed, in principle, by a two or three dimensional stress field solution for the critical zone and sample. Assumption "c" does not appear to vitiate the applications of the theory to uniaxial sample loading failure tests since, as is shown later in this paper, the results obtained are in good agreement with experimental data. The significance of assumption "d", particularly as it pertains to the transition from apparently brittle to ductile failure, is discussed in the next section of this paper.

Failure Criterion for the Critical Zone

Having determined the stress history of the critical zone, it is now necessary to examine the possible modes of failure which the zone may undergo. If the critical zone contained a relatively low molecular weight material, two possible modes of failure could be controlling. The first could involve the cohesive failure of the critical zone by a disruption of the intermolecular bonds between the molecules lying across the potential failure plane. Such failure, which may be termed intermolecular cohesive failure, is similar to the failure exhibited by a cavitating liquid or the shattering of an inorganic glass, and involves little or no intramolecular bond breakdown.

The possibility of a linear high polymer failing in such a manner is remote since the energy or stress required for a cooperative breakdown of the intermolecular bonds along the high polymer chain far exceeds the energy or stress required to sever the covalent bonds in the chain backbone.

Another possible mode of failure for a low molecular weight material could be the viscous translation of the molecules in the critical zone across the

potential failure plane. This viscous mode of failure is also possible for a high polymer and may be the ultimate cause of failure for a ductile or necking type of failure. However, a glasslike high polymer below its glass transition temperature is generally subjected to stress-time-temperature conditions such that apparently brittle failure predominates. The possibility that ductile failure may occur is considered below but, for the present purposes, only apparently brittle failure of the bulk sample is of interest.

It is assumed that the material in the critical zone fails by the dissociation of the primary chain backbone bonds which traverse the potential failure plane (hereafter referred to as active bonds and defined below), when the bulk sample exhibits apparently brittle failure. However, it is recognized that large scale deformations and orientations of the material in the critical zone generally precede the intramolecular bond breakdown in that zone, and are responsible for the apparent differences in failure strengths observed under various sample loading histories, temperatures, and flaw introduction conditions. (A better description of the overall failure process may be had by calling the process semi-ductile rather than apparently brittle but a change in nomenclature at this point would violate the principle of conservation of confusion.)

Thus, regardless of the deformation path by which the critical zone deforms prior to localized failure, a criterion of incipient criticality for the high stress region may be written as follows:

When the tensile stress ($\tilde{t}$) in the critical zone, as defined by the path dependent stress concentration in the critical zone, is such that it equals or exceeds the intramolecular cohesive strength of the average active primary chain bond lying across the potential fracture plane, the critical zone must fail. General material failure must follow if the applied load is not immediately removed or reduced in some fashion.

The nominal stress in the critical zone is given by equation 6, after δ (t) is obtained by simultaneous solution of equations 6 and 7 as outlined above, and may be rewritten as follows:

$$\tau(t) = q_0 \sigma(t) [1+\delta(t)]^{-1/2} \tag{9}$$

where σ(t) is a prescribed, but arbitrary, uniaxial sample loading history.

Let the number of active bonds, per unit area, crossing the potential failure plane in the critical zone be n(t), the volume density of these bonds N(t), and the repeat distance of an active bond measured along the chain backbone be l_b . Then

$$n(t) = N(t) l_b \tag{10}$$

Because the critical zone is highly deformed, prior to incipient criticality, the density of active bonds will decrease as the critical zone grows. Thus

$$\frac{N(t)}{N_0} = [1+\delta(t)]^{-1} \tag{11}$$

where N_0 is the initial volume density of active chain backbone bonds, that is, at time zero and prior to any sample loading history. (Recall that δ (0) = 0.) The number N_0 is therefore the same for bulk and critical zone material. Thus, equations 10 and 11 combine to give

$$n(t) = N_0 l_b [1+\delta(t)]^{-1} \tag{12}$$

It is to be emphasized that equation 11 accounts for the increased volume of the critical zone as a result of its high deformation in the direction parallel to the applied stress. This excess volume may not be uniformly distributed in the critical zone, but rather may be in the form of small pockets or voids, much as

is the case reported for craze structures (22). However, the density correction is required here even though the exact distribution of the added volume is uncertain.

The number average force per active bond in the critical zone is given by

$$F(t) = \frac{\tau(t)\bar{\mu}(t)}{n(t)} \tag{13}$$

where $\bar{\mu}(t)$ is the average cosine projection which the active bonds make with the normal to the failure plane (see figure 4). Combination of equations 9, 12, and 13 gives

$$F(t) = \frac{Q_0 \sigma(t)\bar{\mu}(t)[1+\delta(t)]^{1/2}}{N_0 l_b} \tag{14}$$

Equation 14 may be rearranged as follows:

$$Q_0 \sigma(t)[1+\delta(t)]^{1/2} = \frac{F(t)\bar{\mu}(t)}{N_0 l_b} \tag{15}$$

The maximum permissible value of the right side of equation 15 is obtained when $F(t) = F^*$, the cohesive strength of the active bonds in question, and when $\bar{\mu}$ equals the projection obtained when the molecular chains are completely oriented in the direction of applied stress (see Figure 4). Defining a critical stress function $P_c(t)$ and its maximum value P_c^* as follows:

$$P_c(t) \equiv Q_0 \sigma(t)[1+\delta(t)]^{1/2} \equiv \tau(t)[1+\delta(t)] \tag{16}$$

$$P_c^* \equiv \frac{F^* \bar{\mu}}{N_o l_b} \tag{17}$$

It follows that the condition of incipient criticality is obtained when $P_c(t) = P_c^*$. At all times in the loading history prior to the onset of localized failure, $P_c(t) < P_c^*$.

$$P_c(t) = P_c^* \qquad \underline{\text{Incipient Criticality}} \tag{18}$$

It is to be noted that $P_c(t)$, the critical stress function, is a path-dependent function whose value at any time is determined by the solution to the critical zone rheology-stress concentration problem presented above. This solution will depend upon the sample loading history, the sample's rheological behavior to localized high stress, and parametrically on Q_o, the Neuber constant. It is emphasized that $P_c(t)$ depends on $\sigma(t)$ not only explicitly (see equation 16) but also implicitly through the dependence of $\delta(t)$ on $\sigma(t)$. Furthermore, $P_c(t)$ will, in general, depend on all factors which influence the rheological response of the critical zone such as temperature, strain rate, initial flaw character, etc.

In contrast to $P_c(t)$, the value of P_c^* is solely a function of material constants and represents a local failure criterion which is <u>independent</u> of all rheological manifestations of the failure test. Thus, the value of P_c^* is a material constant and should be applicable to any strain rate, temperature, sample loading history, or initial flaw condition, provided, of course, that apparently brittle failure is the observed mode of sample failure.

In the development of the condition of incipient criticality expressed by equation 18, an active bond refers to a stress-supporting covalent chain backbone bond in a macromolecule which is "anchored" to the glasslike matrix surrounding the critical zone. If such "anchoring" is not highly prevalent, then the critical zone

deformation is not a highly localized deformation of a constant mass of material defined by the original size of the critical zone. Presumably, the anchoring may be accomplished simply by the macromolecule being of sufficient length to completely traverse the critical zone, thereby having both ends imbedded in the glassy matrix. However, it is conceivable that the macromolecule is anchored at one or both ends by partial entaglements with other molecules which partially occupy the critical zone.

Under the appropriate conditions of stress, time, and temperature, the critical zone may grow by the addition of mass, that is, by a collapse of the glasslike walls of the highly stressed region of plastic deformation. If such is the case, then the assumption of a constant mass critical zone process (see the preceding section: The Critical Zone) and equation 11, which gives the volume correction for a constant mass deformation, are not valid. The condition of non-localized and non-confined growth of the critical zone, by mass addition, is believed to represent the onset of general sample ductility. Since the condition of incipient criticality defined by equation 18 represents a maximum stress condition for the material in the critical zone, it follows that a ductile or necking type of failure must occur under conditions such that $P_c(t) < P_c^*$.

At the time-stress-temperature conditions under which sample failure is apparently brittle, the critical stress function path, $P_c(t)$, is such that $P_c(t) = P_c^*$ prior to the stress state and time required for non-localized growth of the critical zone, i.e., for non-confined ductility.

Before proceeding to the numerical application of the theory to PMMA, some qualitative deductions on the effects of temperature may be obtained. Consider a series of samples containing flaws with identical stress concentration factors, i.e., of constant Q_o, which are tested at various temperatures. At the condition of incipient criticality, equations 16, 17, and 18 may be written as follows:

$$\sigma_B \left[1+\delta_B\right]^{1/2} = P_c^*/Q_o \qquad (19)$$

The right side of equation 19 is nearly independent of temperature, since F* and N_o are, at best, weakly dependent on temperature, over a reasonable range. Thus, to a first approximation, P_C* is independent of temperature. However, δ (t) will be a strong function of temperature since it reflects the rheological growth of the critical zone. Given that all samples under consideration have the same Q_o, and hence start with the same stress concentration, rheological considerations dictate that a sample tested at higher temperature will display enhanced viscoelastic-plastic processes within the critical zone. Thus, δ_B is expected to increase with temperature, under identical loading history conditions. It follows directly from equation 19, that σ_B must decrease with temperature.

Thus, the observed decrease of tensile strength with temperature is consistent with the expected enhancement of viscoelastic-plastic response at higher temperatures. By way of contrast, the Griffith equation forces one to conclude that the surface energy term decreases with temperature (refer to equation 1 at constant c) which is contradictory to the supposedly large contribution of plastic processes to the magnitude of the surface energy.

The effect of flaw introduction temperature, at constant tensile test temperature, can be explained as follows: A measure of the initial stress concentration factor for a flaw in a material capable of localized viscoelastic-plastic response is given by the Neuber constant, Q_o, which is proportional to the square root of c/ρ_o. Thus, flaws of identical length have stress concentrations which are inversely proportional to the extent of plastic deformation at the flaw tip. Such considerations led to the experiments summarized in Figures 1 and 2 which show clearly that flaws introduced at a higher temperature are less effective in concentrating stress than flaws introduced at a lower temperature. This observation is

consistent with the expected increase in viscoelastic-plastic deformation processes which would accompany the introduction of a crack (flaw) at a higher temperature.

If the material response to localized high stresses is primarily of an elastic nature, then in the limit of vanishing viscoelastic-plastic deformation at the flaw tip, the critical zone and bulk material approach a homogeneous deformation system, with at best a high gradient of stress near the flaw tip. Under such conditions, it can be shown that this theory approaches, both conceptually and analytically, the Griffith theory. At the other extreme of behavior, where a plastic region of constant size constitutes the critical zone, this theory reduces to Orowan's modification of the Griffith theory. In general, for polymeric glasses, neither extreme of behavior is likely because of the propensity of such systems to undergo localized viscoelastic-plastic deformations which are stress level sensitive. Under these conditions, the time and path dependence of the stress concentration factor is of major importance to a description of the failure process. It is proposed that the theory presented here is at least a first approximation to the phenomenon of the coupled stress concentration - rheological response system.

Theoretical Failure Curves

For PMMA

In order to illustrate the specific applications of the theory, constant strain rate and creep failure of PMMA are considered here. The constant strain rate failure test is an example of a prescribed strain history whereas the creep test represents a prescribed stress history. The rheological model chosen to represent the viscoelastic-plastic response of PMMA is a Maxwell element in series with a Voigt element, the viscous component of which obeys the Eyring hyperbolic-sine flow law. The model is shown in Figure 5, and is described by the following equation:

$$\dot{\epsilon} = \frac{\dot{\sigma}}{k_1} + \frac{\sigma}{\eta} + K \sinh\left\{\alpha\left[\sigma - k_2\left(\epsilon - \frac{\sigma}{k_1} - \int \frac{\sigma dt}{\eta}\right)\right]\right\} \quad (20)$$

If the same model is used to describe the viscoelastic-plastic response of the critical zone, then

$$\dot{\delta} = \frac{\dot{\hat{\tau}}}{k_1} + \frac{\hat{\tau}}{\eta} + K \sinh\left\{\alpha\left[\hat{\tau} - k_2\left(\delta - \frac{\hat{\tau}}{k_1} - \int \frac{\hat{\tau} dt}{\eta}\right)\right]\right\} \quad (21)$$

The model of Figure 5 incorporates the minimum number of required features for the expected rheological response of the critical zone, namely, immediate elastic deformation, viscous flow, and retarded elastomeric response which is highly stress sensitive (activated), the latter through the Eyring viscosity term. In fact, for the rheological constants used for PMMA, the model of Figure 5 shows essentially linear viscoelastic behavior for the bulk material (equation 20) when subjected to constant strain rate loading, whereas the equation for the critical zone (equation 21) with the same constants shows highly viscoplastic response. The latter effect is due to the very high stresses which act in the critical zone which, in terms of the model, serve to drastically lower the effective retardation of the non-linear Voigt element.

Earlier in this paper, it was noted that craze formation, and also critical zone growth, is of an apparently plastic nature. The reason for this qualification is that very high uniaxial orientation and deformation of a high polymeric material, of necessity, produces a restoring force of a conformational entropy origin. Thus, unless the glasslike walls of the critical zone collapse sufficiently to allow large scale mass transfer of chain segments into the critical zone, the restoring force will persist throughout the critical zone history. Because of the very high retardation of the segmental motion processes required to relieve the critical zone, or a craze, of its high deformation, by comparison to the weak conformational entropy restoring force, the deformation will appear plastic within many decades of time after it has occured. Thus, the term apparently plastic is an appropriate description of the critical zone deformation process which, in terms of its influence on the failure properties of polymeric glasses, must be considered truly plastic.

The possibility of appreciable non-localized growth, or viscous flow, of the critical zone has been considered in the previous section of this paper, where it was proposed that such an effect, which did not represent essentially constant mass deformation of the critical zone, may represent the transition to ductile failure. For the present purposes, apparently brittle failure is of interest and thus, the critical zone growth, prior to incipient criticality, is envisaged to be of a nearly constant mass and apparently plastic type. Within the time scale of interest (namely, to failure initiation), the critical zone appears, however, to be of a truly plastic nature. This point of view is consistent with the known structure and behavior of both crazes and fracture surfaces in glasslike high polymers.

The chosen rheological model for the critical zone, equation 21, displays the required behavior. The deformation of the non-linear Voigt element embodies the necessary restoring force whereas the retardation of the Eyring element displays a stress-activated yielding (at the high stresses in the critical zone), but no

such yielding at lower stresses (for example, in the bulk material). Thus, the high deformation of the Voigt element under the influence of a high stress may be associated with the orientation and conformation changes which accompany the growth of the critical zone material. This deformation fits the description of being apparently plastic since a removal of stress would deactivate the Eyring type of flow and result in a "frozen-in" deformation.

Thus, the model of Figure 5 appears to be a good qualitative representation of both the bulk and critical zone response, as is shown below. However, it is again emphasized that the coupled stress concentration-critical zone rheology problem developed in a preceding section of this paper is in no way restricted to a model of the form of Figure 5. As improved rheological descriptions of critical zone material and bulk material become available, the critical zone rheology problem can be embellished accordingly. For the present purpose, the model of Figure 5 is taken to be a first approximation to the behavior of both bulk and highly stressed (critical zone) PMMA, which, needless to say, should give a better description of the path-dependent stress in the critical zone than the constant stress concentration, elastic model of the Griffith type of flaw.

The rheological constants for the model of Figure 5 were obtained by analysis of creep curves on PMMA at the same temperatures to be used in the creep and constant strain rate failure tests. The creep samples were fitted with extensometers which were fed to an oscillographic recorder. The extension record so obtained was used to obtain the immediate elastic deformation of the sample and to insure that the creep load was applied rapidly, but not so rapid as to produce a dynamic stress condition at short times.

The constant k_1 was obtained from the I.E.D. recorded and the known creep load. The constant η was obtained from the long time portion of the creep curve, after the linear creep region had been reached. The value of k_2 was obtained from the total amount of retarded elastomeric deformation observed from the beginning

of the creep test to the limiting value obtained by extrapolation of the linear flow region back to zero time, thereby subtracting out the purely viscous deformation. Finally, the Eyring constants K and α were obtained by a suitable plot of the retarded component of deformation versus log time and comparison of the curve with a series of standard curves obtained from equation 20. Thus, the relative shape of the sigmoidal curve gave α and the position of the curve on the log time axis gave K.

It is emphasized that unique values of all the constants in the model were obtained by the procedure used, and that there was no arbitrary judgment used in obtaining these values. The procedure is explained in detail elsewhere (18). The values of the constants so obtained were checked at various levels of creep stress and found to be consistent. Also, the constants obtained in the creep tests were then used to obtain a constant strain rate stress-strain curve for PMMA, from equation 20, and the predicted curve was in excellent agreement with experimental constant strain rate curves. However, it is to be noted that unique, non-arbitrary values of all the constants of the model cannot be obtained readily from a constant strain rate test.

The constants obtained for PMMA by analysis of creep curves were obtained without any fracture data whatsoever. These constants are tabulated in Table 1 for PMMA at 35°C and are used in the critical zone rheology analysis below for both the constant strain rate and creep failure theoretical curves. No adjustments or modifications of the constants are used in the analysis for various loading histories, flaw introduction temperatures, or rate of loading effects, provided of course that all the failure tests are to be performed at the same temperature, namely 35°C. For other temperatures or environmental conditions, new rheological constants are necessary for the particular conditions of interest.

One way to proceed with the analysis of the path dependent stress concentration in the critical zone, for a rheological equation of the form of equation 21,

Table 1

Rheological Constants for PMMA at 35°C

$k_1 = 3 \times 10^{10}$ dynes/cm^2

$k_2 = 3 \times 10^{10}$ dynes/cm^2

$\eta = 1 \times 10^{16}$ dyne-sec/cm^2

$\alpha = 3 \times 10^{-8}$ cm^2/dyne

$K = 5 \times 10^{-9}$ sec^{-1}

is to eliminate the stress τ and its derivatives from this equation by means of equation 6. Thus, from equation 6:

$$\tau = q_0 \sigma(t) [1+\delta(t)]^{-1/2} \tag{6}$$

$$\dot{\tau} = q_0 \left\{ \dot{\sigma}(t) [1+\delta(t)]^{-1/2} - \frac{\sigma(t)\dot{\delta}(t)}{2[1+\delta(t)]^{3/2}} \right\} \tag{8}$$

$$\ddot{\tau} = q_0 \left\{ \frac{\ddot{\sigma}(t)}{[1+\delta(t)]^{1/2}} - \frac{\dot{\sigma}(t)\dot{\delta}(t)}{[1+\delta(t)]^{3/2}} - \frac{\sigma(t)\ddot{\delta}(t)}{2[1+\delta(t)]^{3/2}} + \frac{3\sigma(t)[\dot{\delta}(t)]^2}{4[1+\delta(t)]^{5/2}} \right\} \tag{22}$$

Combination of equations 6, 8, and 22 with equation 21 and rearrangement and inversion of the hyperbolic sine term give, after differentiation of equation 21 to remove the integral sign:

$$\ddot{\delta}(t) = \left\{ q_0 k V [\ddot{s} - V^2 \dot{s}\dot{\delta} + \tfrac{3}{4} V^4 s(\dot{\delta})^2] + \frac{q_0 k_2 z_1}{\eta} + k_2 K \alpha [q_0 z_1 + z_2] \left[\left(\frac{z_2}{K}\right)^2 + 1 \right]^{1/2} \right\} \left\{ 1 + \frac{5 V^3 q_0 k}{2} \right\}^{-1}$$

where $z_1(t) = v\dot{s} - v^3 s \dot{\delta}/2$

$$z_2(t) = Q_0 k z_1 + \frac{Q_0 k_2 s v}{\eta} - \dot{\delta}$$

$$s(t) = \frac{\sigma(t)}{k_2}$$

$$v(t) = [1+\delta(t)]^{-1/2} \qquad k = k_2/k_1$$

Because of the particular form for the critical zone rheological equation, equation 21, the stress σ and its derivatives occur in equation 23 always divided by k_2. Thus, it is convenient to define a dimensionless applied stress $S = \sigma/k_2$.

The non-linear, rather complex form of equation 23 for the critical zone size is not due entirely to the rheological equation form chosen for analysis, namely equation 21. It is easily shown that if the rheological equation for the critical zone were simply a Maxwell equation, $\dot{\tau}/k + \tau/\eta = \dot{\delta}$, then the equation obtained after elimination of the critical zone stress (the equivalent of equation 23 here) would also be non-linear in δ. This is because the critical zone stress τ and its size δ are not linearly coupled (see equation 6). Thus, the path-dependent stress concentration problem is inherently of a non-linear nature, regardless of the rheological equation which describes the critical zone. This is due to the form of the stress concentration factor, equation 6, which must be considered when plasticity effects are present at the flaw site.

Using the constants for PMMA, as tabulated in Table 1, equation 23 may be solved numerically to obtain δ (t), for any prescribed stress history σ(t), and parametrically as a function of Q_o. For the constant strain rate condition, the bulk strain history is given by $\epsilon = rt$ (for all $t \geq 0$) where r is a constant rate of strain. Equation 20 can now be solved numerically to obtain σ(t), $\dot{\sigma}$ (t), $\ddot{\sigma}$ (t) corresponding to the chosen strain history. Thus, a numerical solution to the non-linear differential equation for the critical zone size, equation 23, can now be

performed, thereby yielding $\delta(t)$ for a specified Neuber constant Q_o, and for the chosen stress (strain) history.

(The procedure is somewhat more straightforward if the sample stress history is prescribed, since $\sigma(t)$ and its derivatives are known directly. Therefore, use of equation 20 to generate $\sigma(t)$ and its derivatives from a prescribed strain history $\epsilon(t)$ is not required).

The analysis described above has been carried out for PMMA at various rates of strain, through the use of a high speed computer and a fourth order Runge-Kutta scheme for the second order equation for the critical zone, equation 23. The rate of growth of the critical zone, $\dot{\delta}(t)$, obtained for a particular set of conditions is shown in Figure 6, where the stress activated yielding of the rheological model is clearly evident. Another integration of $\dot{\delta}(t)$ gives $\delta(t)$ which can be used with the known (prescribed) sample stress $\sigma(t)$ to generate the critical stress function $P_c(t)$ (see equation 16). Figure 7 shows the final results of the calculations for the critical stress function $P_c(t)$ as a function of time, for various Neuber constants, and for a constant sample strain rate of 10^{-3} sec.$^{-1}$. Such curves are obtainable for any arbitrary, but prescribed, sample stress or strain history, and for any arbitrary critical zone rheological equation (for example, equation 21).

The critical stress function paths shown in Figure 7 are, in general, a function of the Neuber constant (initial stress concentration factor), the environmental conditions as they affect the rheological constants of the critical zone, the sample stress or strain history (in this case, constant strain rate), and the particular constitutive equation which describes the critical zone behavior in the given material.

The criterion of incipient criticality, as given by equation 18, can now be applied to the results shown in Figure 7. For PMMA, the constants used in the evaluation of P_c^*, from equation 17, are obtained as follows: It is assumed that the

carbon-carbon backbone bond can be described adequately, in tension, by the Morse potential, equation 24.

$$U = U_o\left[1 - \exp(-a)\left(\frac{l - l_e}{l_e}\right)\right]^2 \qquad (24)$$

where U is the bond energy at a spacing l, U_o is the bond dissociation energy, "a" is a constant obtainable from spectroscopic data, and l_e is the equilibrium bond spacing.

The bond "force constant" is given by the second derivative of the bond energy, d^2U/dl^2. At bond spacings greater than the spacing where the Morse potential exhibits an inflection, the force constant is negative. Thus, the inflection point represents, in a classical sense, the dissociation point for the bond. The maximum value of the force which the bond can support, i.e., its cohesive strength, is obtained by evaluation of the first derivative of the Morse potential at the point of inflection, which yields equation 25.

$$F^* = \frac{|U_o|\,a}{2 l_e} \qquad (25)$$

Using known values of the Morse constants for the carbon-carbon bond (23), as follows:

$$a = 3.35$$
$$|U_o| = 5.5 \times 10^{-12} \text{ ergs/bond}$$
$$l_e = 1.57 \times 10^{-8} \text{ cm.}$$

the cohesive strength is calculated to be

$$F^* = 5.87 \times 10^{-4} \text{ dynes/bond} \qquad (26)$$

For PMMA, the molecular weight of a repeating unit is 100, and the density of the bulk material is 1.18 to 1.19 at 25°C (24). The number of active bonds per repeat unit is two. Therefore, N_o (see equation 17) is given by equation 27.

$$N_o = \frac{2(1.18)\ (6.02 \times 10^{23})}{100} \qquad (27)$$

Referring to the derivation of equation 17 and Figure 4, l_b is taken to be the length of the carbon-carbon bond (1.57 Å), and $\bar{\mu}$ is given by equation 28 for complete orientation of the critical zone material at failure.

$$\bar{\mu} = \text{cosine}\ \frac{(180 - 109.5)}{2} = 0.81 \qquad (28)$$

Combination of equations 17, 26, 27, and 28 gives

$$P_c^* = 1.62 \times 10^{11} \frac{\text{dynes}}{\text{cm}^2} \text{ or } \frac{P_c^*}{k_2} = 5.40 \qquad (29)$$

Since the particular form of equation 23 led to the convenient dimensionless applied stress $S = \sigma/k_2$, the ordinate of Figure 7 is plotted as dimensionless $P_c(t)/k_2$. Thus, the value of P_c^* can also be made dimensionless by the same constant k_2, as indicated in equation 29. This simply corresponds to division of both sides of the failure criterion, equation 18, by the constant k_2.

Referring to Figure 7, incipient criticality of the critical zone, and thereafter apparently brittle sample failure, occurs when the critical stress function reaches the horizontal line which denotes $P_c^*/k_2 = 5.40$. This corresponds to the failure criterion given by equation 18. Again, it is emphasized that the critical stress function path $P_c(t)$ will, in general, depend on the rheological response of the critical zone, the environmental conditions, the sample loading history, and the initial stress concentration factor, as given by the Neuber constant (Q_o). However, for a given material, P_c^* represents a material constant independent of the rheological response of the critical zone. Thus, the value of $P_c^* = 1.6 \times 10^{11}$ represents the criticality condition for apparently brittle failure of PMMA regardless of the nature of the sample loading history, environmental conditions, or Neuber constant.

For the constant strain rate condition used to generate the critical stress functions of Figure 7, the intersections of the curves of various initial stress concentration factors with the horizontal criticality curve give the times to failure for the various Neuber constants. Since the stress (or strain) history applied to the sample is specified, the time to failure immediately gives the sample stress (or strain) at failure. Thus, a plot of failure stress versus Neuber constant is readily obtained and these results are shown in Figure 8. Also shown in this figure are results obtained for different sample strain rates, after development of the appropriate critical stress functions in a manner identical to that used to obtain Figure 7. The effect of a two decade change in strain rate is small, but is consistent with experimental observation (25).

Calculations for a sample stress history which corresponds to a rapid rate of stress followed by a constant creep load have been performed in detail elsewhere (18) where an asymptotic formula for creep failure is also presented. The creep failure calculations are summarized here in Figure 9, for PMMA at 35°C. The method of solution is identical to that used to obtain Figure 8, namely solution for the critical zone growth, equation 23, followed by calculation of the critical stress function, both for a creep stress history (σ_o) applied to the sample. Finally, the criterion of incipient criticality, equation 18, was used to obtain the final results, Figure 9.

Because of the particular form of equations 21 and 23 which describe the critical zone rheological response, the creep results are plotted in Figure 9 with an ordinate given by S_oQ_o ($= \frac{\sigma_o Q_o}{k_2}$). The constant k_2 is known (see Table 1) and Q_o represents the Neuber constant, or initial stress concentration factor, for a given creep sample. If a series of samples are chosen for creep failure study which all have similar adventitious or artificial flaws, then Q_o merely corresponds to a vertical scale expansion factor in Figure 9, from which a creep failure curve of σ_o versus log t_B (time to break) can be readily obtained.

Further discussion of the theoretical failure results obtained by the critical stress function analysis for the critical zone is presented below after comparison of Figures 8 and 9 with experimental failure data.

Experimental Applications

To PMMA

The theoretical failure curves developed for constant strain rate (Figure 8) and creep (Figure 9) failure of PMMA at 35°C can be applied directly to experimental data on the fracture of this material under the same conditions. Experimental studies were performed on cast PMMA sheet (Rohm & Haas, Plexiglas II, Type G) of one-sixteenth inch nominal thickness. The fracture samples and the samples used in the creep study to obtain the rheological constants for equations 20 and 21 (see Table 1) were cut from the same sample sheets.

The experimental procedure for sample preparation is described in detail elsewhere (18). Briefly, sample blanks were cut from the PMMA sheet and artificial flaws in the form of edge cracks were introduced by means of a razor blade guillotine enclosed in a constant temperature chamber. Samples were discarded if the free running crack produced was not perpendicular to the sample edge, or if the free running crack was not appreciably longer than the initial razor blade penetration. Final sample machining was performed on a high speed "Tensil-Kut" machine. The creep samples were machined to a rectangular shape of six inches by one-half inch, and the constant strain rate samples conformed to ASTM specification D638-58T. After machining, the flaw sizes (free running crack length) were measured on a polarized light microscope. The samples were then loaded to failure using an "Instron" tensile tester for constant strain rate tests, or a creep tester for the creep load failure tests. The construction and operation of the creep tester is described in detail elsewhere (18). All tests were performed at constant temperature.

The results for a constant strain rate of 10^{-3} sec.$^{-1}$, and at 35°C, are shown

in Figure 10 where the logarithm of the breaking stress is plotted versus the logarithm of the artificial flaw (crack) length. In Figure 11 the creep failure results are plotted as the logarithm of the creep load times the square root of the flaw (crack) size (multiplied by a constant) versus the logarithm of the time to failure. The data of Figure 11 include all combinations of creep load and flaw size, e.g., large flaw-small load, and small flaw-large load. The data presented were all obtained at 35°C on samples containing artificial flaws introduced at 25°C. The effect of flaw introduction temperature has already been emphasized and Figures 1 and 2 show the least-mean-squares lines for data obtained in the same manner as the data of Figure 10.

In order to compare the experimental results with the theoretical failure curves, it is necessary to first consider the effect of crack length on the initial size of the critical zone. For flaws introduced under controlled conditions of crack introduction, it is to be expected that the initial size of the critical zone, ρ_o, is independent of the length of the crack, c. This would be the case if all the cracks were free running and introduced at the same temperature. Thus, it is proposed that ρ_o is a constant for a series of samples containing artificial flaws of various length, but all introduced under identical cracking (flaw introduction) conditions. However, ρ_o is a function of the particular flaw introduction technique and/or conditions, for any given material.

These deductions are intuitively appealing, when one considers the physical significance of the initial state of the critical zone. However, these deductions are essentially confirmed, or at least shown to be consistent, with the quantitative predictions of the theory. It is well known that a plot of $\log \sigma_B$ vs. $\log c$ for constant strain rate failure of PMMA or PS gives a straight line of slope (-1/2). Figure 8 also gives a straight line of slope (-1/2) when $\log \sigma_B$ is plotted vs. $\log Q_o^2$ (recall that $Q_o^2 \sim \frac{4c}{\rho_o}$). Thus, artificial flaw introduction techniques do indeed result in ρ_o being independent of flaw length c, but dependent on the

conditions of flaw introduction, as is experimentally verified by Figures 1, 2, and 10. Note that the difference of log Q_o^2 and log c is equal to log $4/\rho_o$ and is independent of flaw length for any given flaw introduction temperature, all other flaw introduction variables such as propagation velocity being held constant (in this case, all being free running edge cracks).

The theoretical failure curves of Figures 8 and 9 were calculated without recourse to fracture data of any kind. The only parameters used were known bond strength and density constants for the PMMA chain backbone and rheological constants obtained from creep tests. Therefore, since artificial flaws were used in the experimental failure studies whose lengths were measured prior to the test, it follows that ρ_o is the only undetermined parameter in Figures 8 and 9. However, the physical meaning of ρ_o is definite. Since the experimental failure data of Figures 10 and 11 were performed on samples containing flaws of known length, it follows that comparison of Figures 8 and 9 with Figures 10 and 11, respectively, should yield theoretical ρ_o values, for the particular flaw introduction conditions used.

Since ρ_o has been shown to be independent of flaw length, but dependent on flaw introduction conditions, and since the flaws in both the constant strain rate and creep failure samples were introduced under identical conditions, it follows that ρ_o for both Figures 10 and 11 should be the same. This is a necessary condition on the internal consistency of the theory and its applicability to various sample loading histories.

Comparison of Figures 8 and 10 shows that the abscissae of these graphs differ by a horizontal shift factor of log $(4/\rho_o)$. In Figure 10, the experimental data are represented by points whereas the solid line is actually the theoretical failure curve of Figure 8 shifted horizontally. The shift factor used corresponds to a ρ_o value of 190 Å, which corresponds to the initial critical zone size for the given flaw introduction conditions.

Similarly, comparison of Figure 9 (replotted with a logarithmic ordinate) and Figure 11 shows that the ordinates differ by a factor of $[\log(\rho_o)^{1/2}+3]$. In Figure 11, the solid line is actually the theoretical curve of Figure 9 shifted vertically by an amount which corresponds to a ρ_o value of 120 Å, at the given flaw introduction conditions.

In view of the admittedly crude first approximation to the critical zone rheological response, as given by equation 21, the agreement of the values of ρ_o obtained independently from both creep and constant strain rate failure tests is deemed quite satisfactory. Moreover, the internal consistency of the concepts on which the theory is predicated, when applied to variations of strain rate, test temperature, flaw introduction temperature, and sample loading history leads us to believe that these concepts are basically correct. Furthermore, the shapes of the theoretical creep failure curve and the constant strain rate failure curve are in agreement with experimental data.

The theoretical failure curve of Figure 9 indicates a marked decrease of creep stress with failure time at about 10^6 seconds. There is some indication that the experimental data of Figure 11 tend to verify this effect predicted by the theory. However, additional creep failure data at small flaw size and load conditions are required to establish the validity of this predicted deviation from the often used, but empirical, linear relationship between creep stress and log (time-to-break).

The dependence of ρ_o on the flaw introduction temperature for PMMA can be obtained by comparison of Figures 1 and 8 using the horizontal shift calculation described above. The results of these calculations are presented in Table 2.

Table 2

Effect of Flaw Introduction Temperature on the Initial Size of the Critical Zone in PMMA (all samples fractured at 35°C.)

Flaw Introduction Temperature (°C)	ρ_o (Å)
-70	177
30	195
55	239

The variation of ρ_o with flaw introduction temperature is as expected, in that higher temperatures should result in enhanced viscoelastic-plastic deformation, thereby resulting in less effective stress concentrations for a given flaw length.

Discussion

The theoretical failure curves of Figures 8 and 9 are two examples of the application of the theory to various sample loading histories. Both the constant strain rate and creep failure curves were constructed using the same rheological constants for the critical zone response and, of major importance, the same failure criterion for the critical zone. Differences in failure strengths, or times to failure, which result from variations in sample loading history, initial flaw character or method of introduction, and temperature all serve to alter the path dependence of the critical stress function $P_c(t)$. In contrast to the path dependence of $P_c(t)$, the critical stress number P_c^* is a material constant independent of all rheological manifestations and responses within the critical zone and is therefore a true criterion of local failure initiation provided, of course, that apparently brittle failure is the mode of fracture.

The criterion of incipient criticality, or local failure, as given by P_c^*, requires a knowledge of the strength, density, and orientation of the chain backbone bonds which ultimately fail within the critical zone. It is easily shown, in fact, that the same parameters are involved in theoretical estimates of γ, the Griffith surface energy. However, because the coupled stress concentration-critical zone rheology problem is directly formulated in terms of the stress which acts within the critical zone, the failure criterion is conveniently expressed as a critical stress rather than a critical surface energy. This avoids the paradoxical

definition of a surface energy which is a path-dependent variable but is supposed to represent a material constant.

Referring to equation 19, it can be shown that the theoretical curve of Figure 8 would not give a straight line unless the factor $(1+\delta_B)^{1/2}$ is <u>independent</u> of the Neuber constant Q_θ. In the development of Figure 7 for the critical stress function $P_c(t)$, it was necessary to solve for the relative growth of the critical zone as a function of time, namely $\delta(t)$, when the critical zone was subjected to a <u>variable</u> stress concentration factor which itself is a function of δ. As shown earlier, this required the formulation and solution of equation 23 (for the chosen example, rheological equation 21). Thus, $\delta(t)$ at the time of incipient criticality, namely the intersection of $P_c(t)$ with P_c^* in Figure 7, is also obtained during the procedure used to construct Figure 7 (or its equivalent for any sample loading history).

For the conditions of Figures 7 & 8 (namely, PMMA; at 35°C; under a constant strain rate loading; and for the critical zone rheological response specified by equation 21 and the constants of Table 1), the values of $\delta(t)$ at failure initiation (i.e., δ_B) obtained are given in Table 3.

Table 3

Theoretical Values of Critical Zone Growth to Failure for PMMA Under Constant Strain Rate at 35°C.

Strain Rate (sec^{-1})	Q_o	$\delta_B = \frac{\rho_B - \rho_o}{\rho_o}$
1×10^{-4}	250	2.814
	500	2.813
	1000	2.811
	2000	2.808
1×10^{-3}	250	2.813
	500	2.812
	1000	2.791
1×10^{-2}	250	2.812
	500	2.810
	1000	2.790
	2000	2.786

The theoretical calculations show that the critical zone relative growth from the initiation of loading to the instant at which flaw propagation initiates is essentially independent of the initial stress concentration factor, for a constant strain rate loading at a given temperature. This is so even though the $\delta(t)$ path is definitely dependent on the Neuber constant. The tensile test temperature should have a far greater influence on the value of δ_B than the effect of strain rate, presumably because of the strong influence of temperature on the rheological constants for the critical zone. However, calculations at temperatures other than 35°C are required to substantiate this effect.

In view of the constancy of δ_B versus Neuber constant, for a constant strain rate loading, it can be concluded that glasslike

high polymers give qualitative agreement with a Griffith type plot of $\log\sigma_B$ versus log c for two reasons: (1) The value of ρ_o is essentially independent of flaw length provided all flaws are introduced under identical conditions. (2) The total growth of the critical zone up to the initiation of flaw propagation is essentially independent of the level of initial stress concentration. However, it is conceivable that a glasslike high polymer with rheological response to localized high stress of a nature considerably different than that described by equation 21 would not result in constancy of δ_B. Under such conditions, the equivalent of Figure 8 would not be a straight line.

The theoretical values of δ_B can be used to obtain a measure of the size of the critical zone at the instant of flaw instability. If $\rho_o = 195\text{Å}$, and δ_B is taken as 2.8, then $\rho_B = \rho_o(1+\delta_B) = 740\text{Å}$. The total thickness of the critical zone is 2ρ, or ca. 1500Å.

Since the stress is a maximum at the flaw tip in the apparently plastic zone and decays outward from the flaw tip, plasticity effects will be most pronounced at the flaw tip. The numerical value of ρ characterizes the maximum stress at the flaw tip, and may be thought of as representative of the size of a truly plastic zone with a uniform stress equal to the maximum stress at the flaw tip. Therefore, numerical values of ρ at any instant of time (e.g. ρ_B) must be numerically smaller than the extent of plastic deformation at the flaw tip in any material capable of apparently plastic response. This is the case because the viscoelastic-plastic deformation at the flaw tip is a result of the cumulative effect of the entire stress history which existed at the flaw vicinity, as well as the instantaneous stress level.

Summary

In the introduction, attention was called to the Orowan treatment for a crack blunted by a plastic domain. However, the conclusions reached here appear to be more general in that consideration has been given to a general viscoelastic-plastic zone which generates a time-and path-dependent stress concentration factor. The theoretical predictions are consistent with both Griffith's and Orawan's treatments when applied to constant strain rate data for glasslike polymers. In addition, the present theory provides an explanation of several conceptual difficulties which arise in the application of the Griffith surface energy concept.

(a) The effect of flaw introduction temperature is consistent with the physical interpretation of the critical zone, prior to flaw instability.

(b) The effect of a change in strain rate is predicted, a priori, without recourse to an ad hoc variation in the failure criterion.

(c) The "inherent flaw size" concept (3) developed from data on samples containing both adventitious and artificial flaws has shown anomolous behavior in that the inherent flaw size appears to vary with temperature. In terms of the present theory, the procedure used to obtain the inherent flaw size cannot be considered valid since it has been shown that flaw introduction conditions produce flaws of different initial stress concentrating ability. Thus, adventitious and inherent flaws cannot be characterized with respect to flaw length alone.

(d) The variation of tensile strength with temperature is consistent with the expected enhancement of viscoelastic-plastic response in the critical zone and does not require any modification of the criterion of local failure.

(e) For a given material with known rheological constants, and known molecular chain backbone structure, theoretical failure curves for arbitrary sample loading histories can be predicted, a priori, and depend only on the initial stress concentrating ability of the critical flaw. The criterion of local failure, or flaw instability, is a material constant which is independent of the rheological response at the critical flaw tip.

Acknowledgements

The contents of this paper are taken, in part, from a thesis submitted to the Department of Chemical Engineering, Rensselaer Polytechnic Institute, in partial fulfillment of the requirements for the Doctor of Philosophy degree (18).

The authors wish to express their appreciation to the Institute of Paper Chemistry for a Pioneering Research Grant which supported this work. Partial student support in the form of an N. D. E. A. Fellowship is also acknowledged.

This work was performed in the Rensselaer Materials Research Center, Polymer Research Laboratories, which are partially supported by the National Aeronautics and Space Administration.

References

1. Griffith, A. A., Phil. Trans. of the Royal Soc. A-221, P. 163, (1921).

2. Berry, J. P. and A. M. Bueche, G.E. Research Report 61-RL-(2812c), Aug. (1961).

3. Berry, J. P., "General Theory of Brittle Fracture," section II A, and "Brittle Behavior of Polymeric Solids," section II B in Fracture Processes in Polymeric Solids edited by B. Rosen, Interscience, New York, (1964).

4. Berry, J. P., J. Polymer Sci. 50, p. 107; P. 313, (1961).

5. Higuchi, M., Reports Research Inst. Appl. Mech. (Japan) 6, P. 173, (1958).

6. Wolock, J., J. A. Kies, and S. E. Newman, Fracture, P. 250, John Wiley, New York, (1959).

7. Berry, J. P., Nature 185, P. 91 (1960); J. Appl. Phys. 33, p. 1741, (1962); J. Appl. Phys. 35, P. 1355 (1964).

8. Kambour, R. P., J. Polymer Sci. 3, P. 1713, (1965).

9. Kambour, R. P., J. Polymer Sci. (A2) 4, P. 17, (1966).

10. Kambour, R. P., J. Polymer Sci. A2, P. 4165, (1964).

11. Berry, J. P., J. Polymer Sci. A1, P. 995, (1963).

12. Cessna, L. C., Jr. & S. S. Sternstein, Polymer Letters (J. Polymer Sci.) 3, P. 825, (1965).

13. Huffman, G. M., "Viscoelasticity in the Fracture of Polymer Solids: Polystyrene Below Its Glass Transition Temperature," Masters Thesis, Dept. Chemical Engineering, Rensselaer Polytechnic Institute, Troy, N. Y., Sept. 1966.

14. Neuber, H., Kerbspannungslehre, P. 142, Julius Springer, Berlin, (1937). Translation available from David Taylor Model Basin, Navy Dept., no. 74.

15. Barenblatt, G. I., Advances in Applied Mechanics 2, P. 55, Academic Press, New York (1962).

16. Orowan, E., J. of Welding (Research supplement) 34, (1955).

17. Bikerman, J. J., S.P.E. Trans. 4, P. 250, (1964).

18. Cessna, L. C., Jr., "The Fracture of Polymers Below Their Glass-Transition Temperatures," Doctoral Dissertation, Dept. Chemical Engineering, Rensselaer Polytechnic Institute, Troy, N. Y., April, 1965.

19. Cessna, L. C. and S. S. Sternstein, Fracture in Glasslike High Polymers: I. Theoretical Considerations; II. Applications to PMMA, to be published.

20. Sternstein, S. S., and K. Sims, "Propagation Rates and Fracture Morphology of Solvent Induced Single Crazes,: A.C.S. Polymer Preprints 5, Sept. (1964).

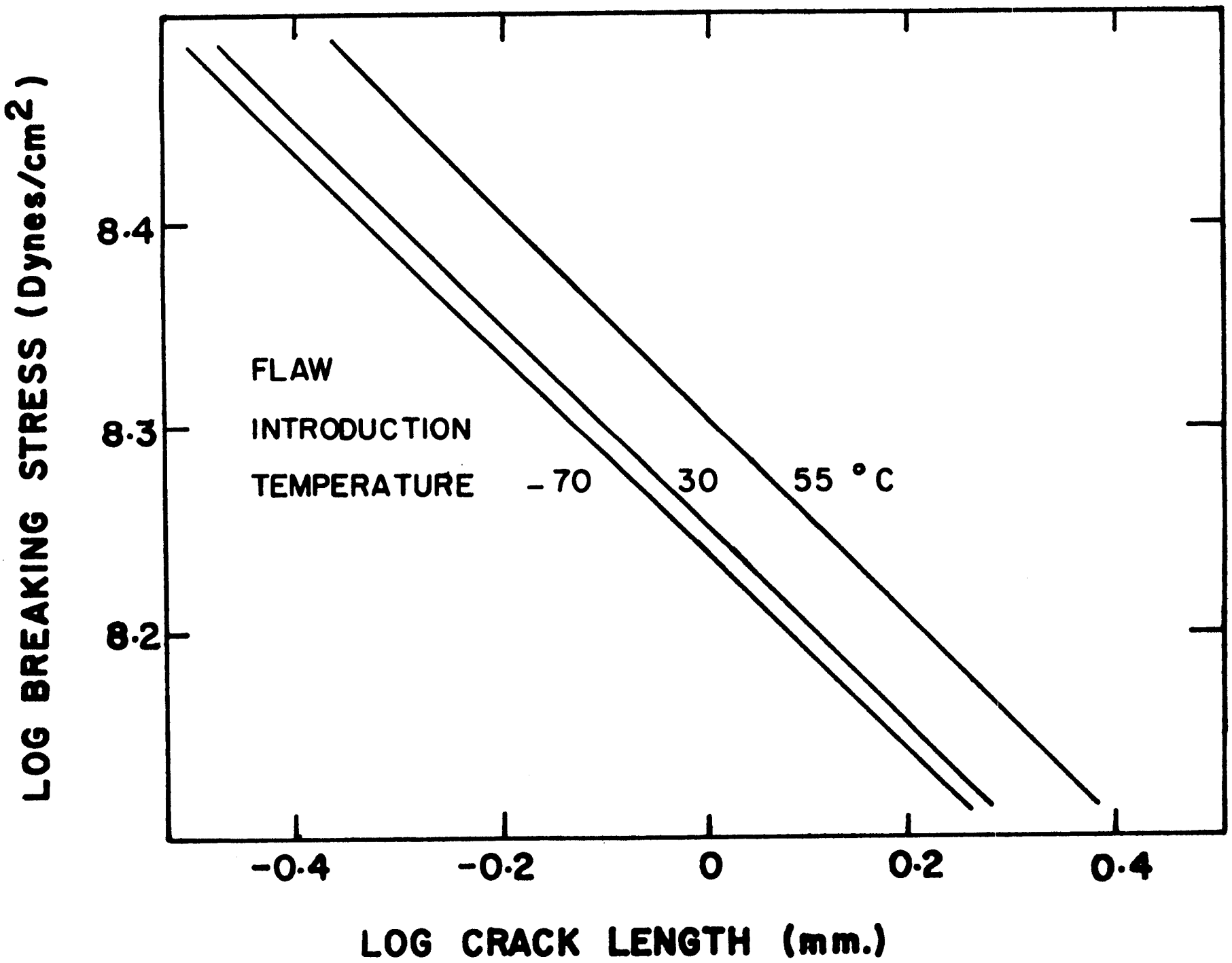
LOG BREAKING STRESS (Dynes/cm^2)
8·4
8·3
8·2
FLAW
INTRODUCTION
TEMPERATURE
-70
30
55 °C
-0·4
-0·2
0
0·2
0·4
LOG CRACK LENGTH (mm.)

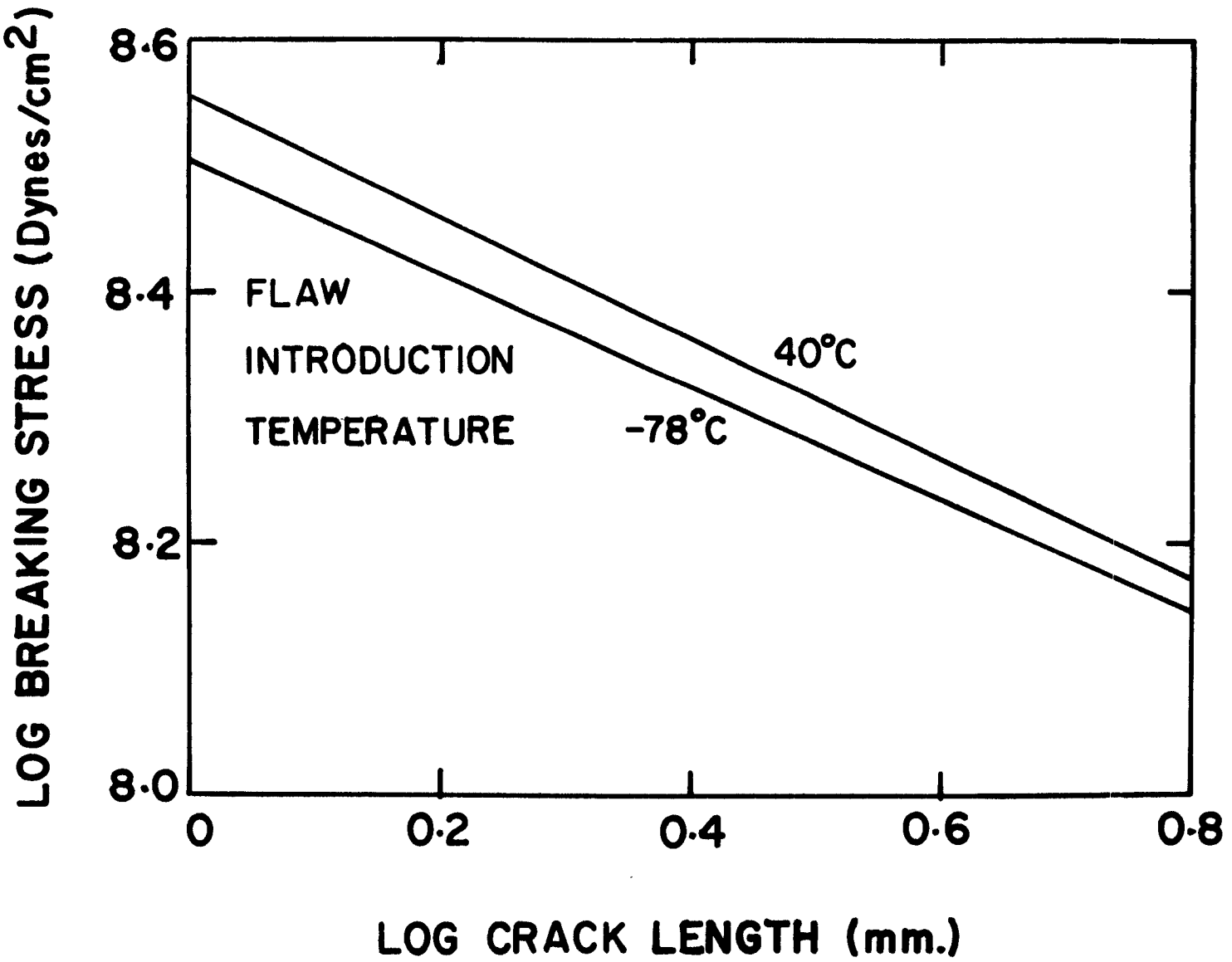
LOG BREAKING STRESS (Dynes/cm2)
8·6
8·4
8·2
8·0
FLAW
INTRODUCTION
TEMPERATURE
40°C
-78°C
0
0·2
0·4
0·6
0·8
LOG CRACK LENGTH (mm.)

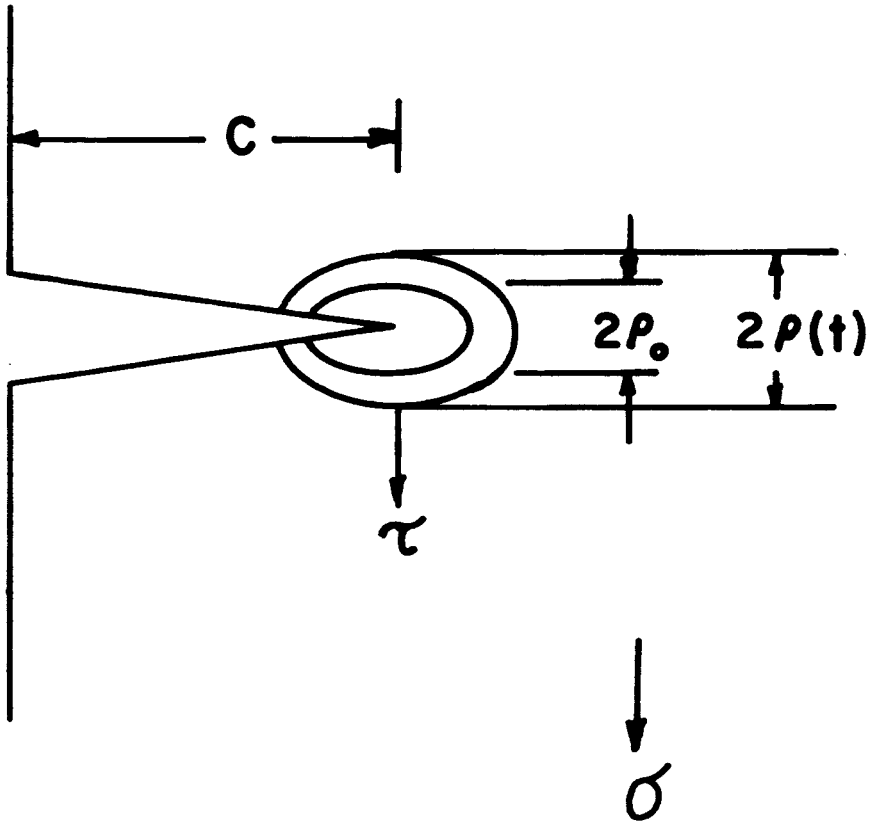
C
2ρ₀
2ρ(t)
τ
σ

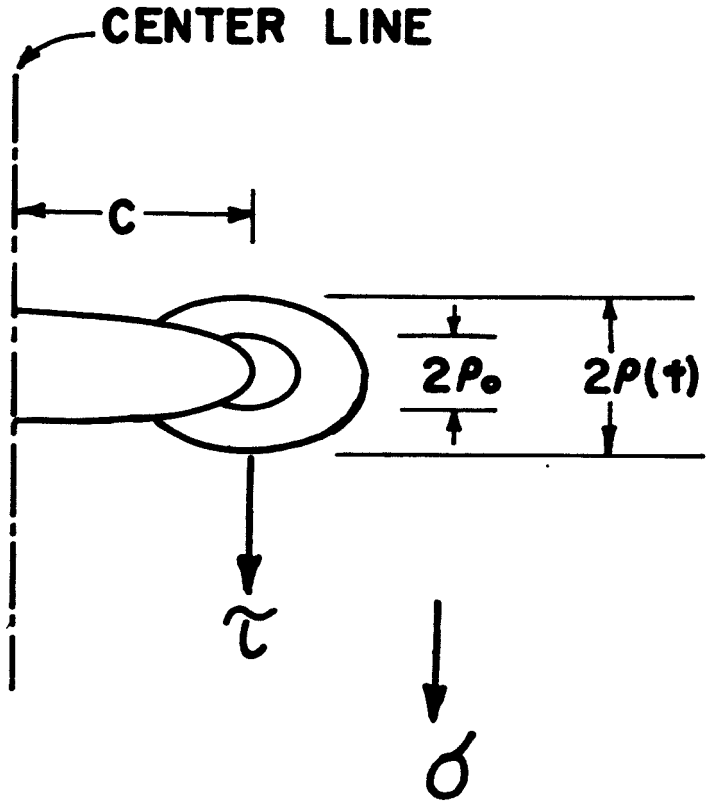
CENTER LINE
C
2ρ₀
2ρ(t)
τ
σ

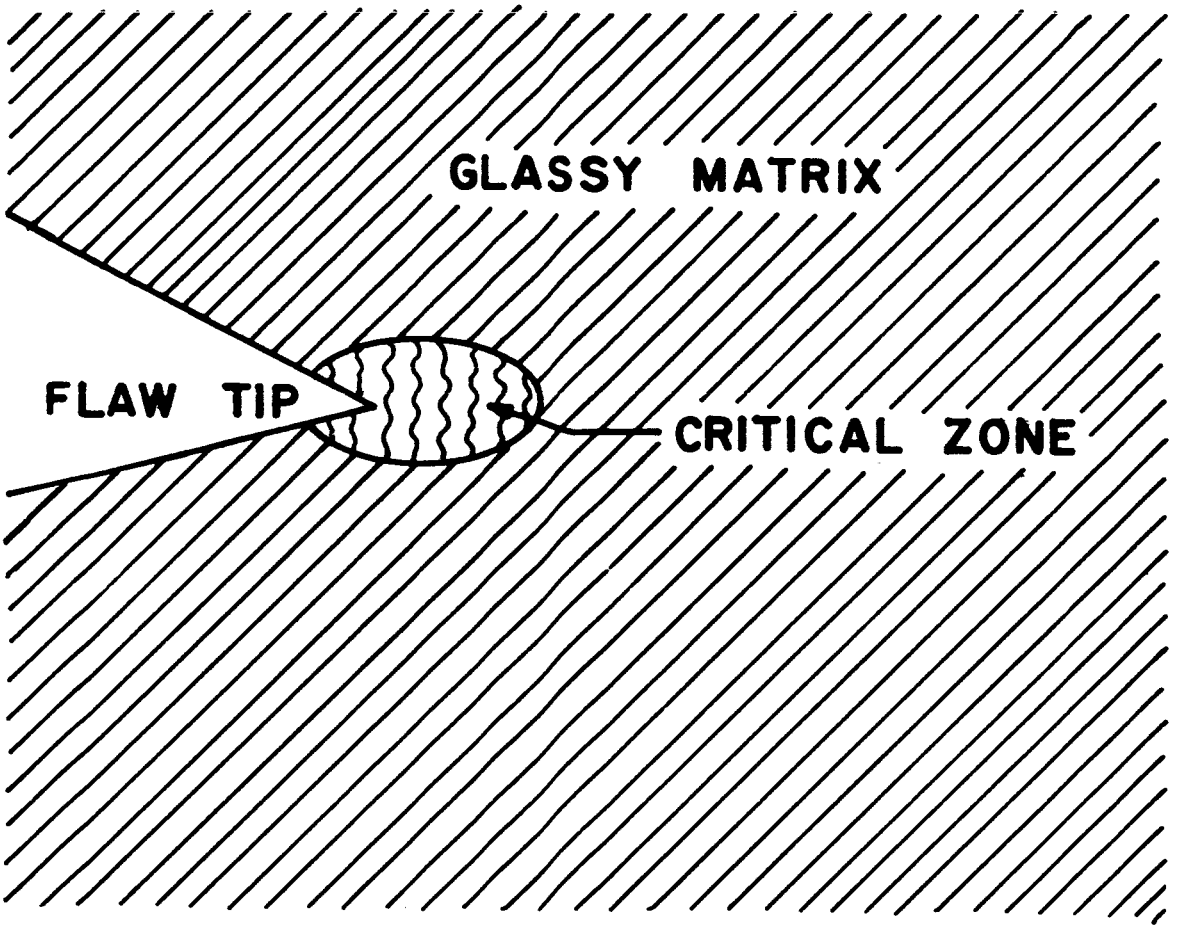
GLASSY MATRIX
FLAW TIP
CRITICAL ZONE

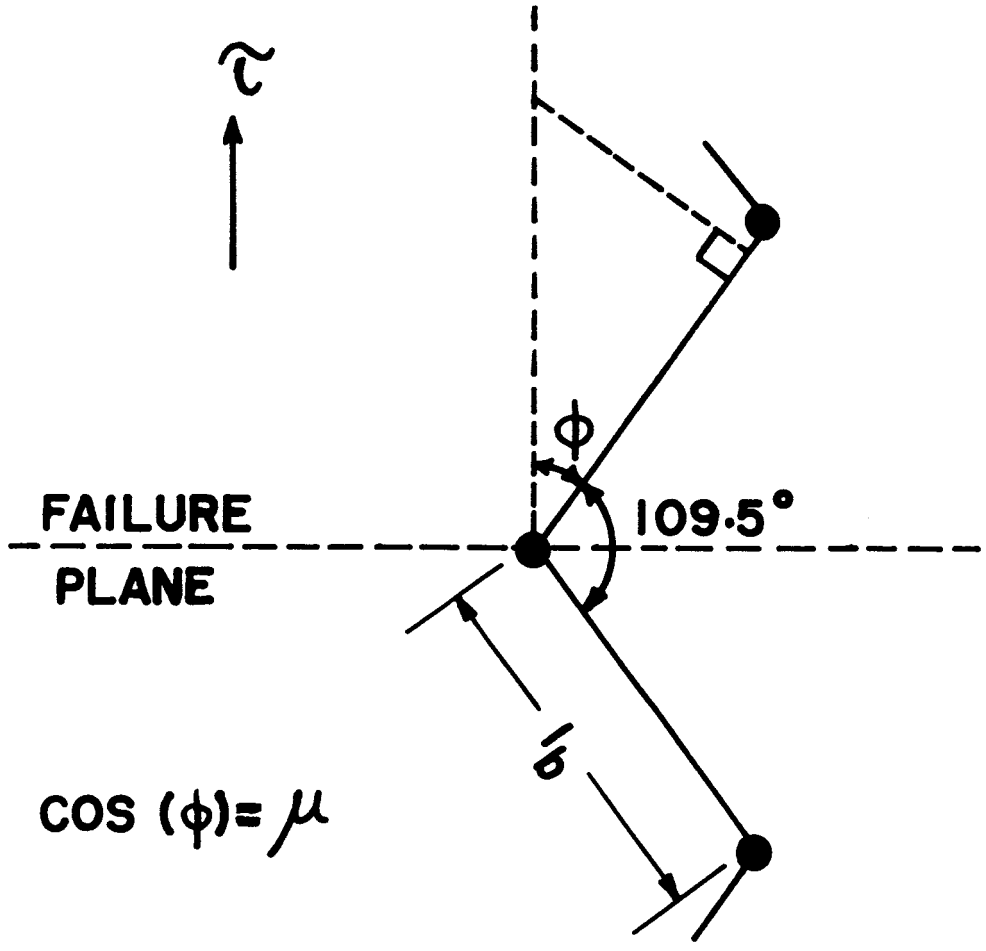
τ
FAILURE
PLANE
Φ
109·5°
σ
COS (Φ)= μ

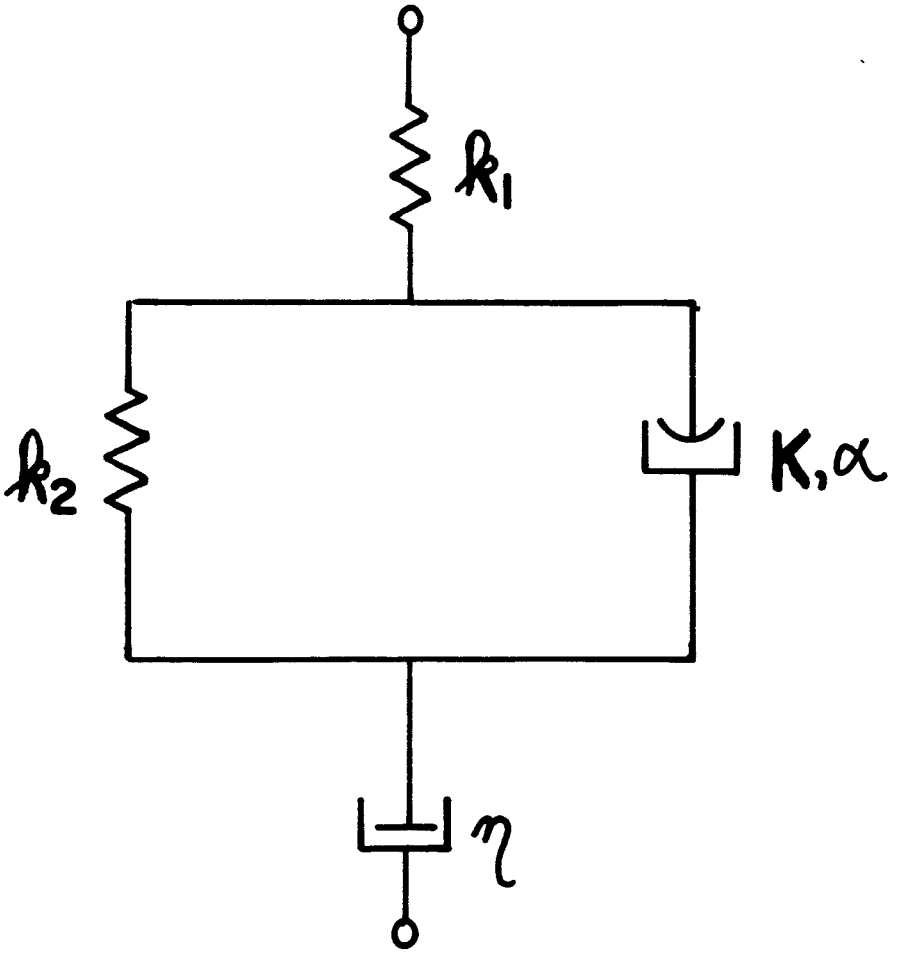
k_1
k_2
K, α
η

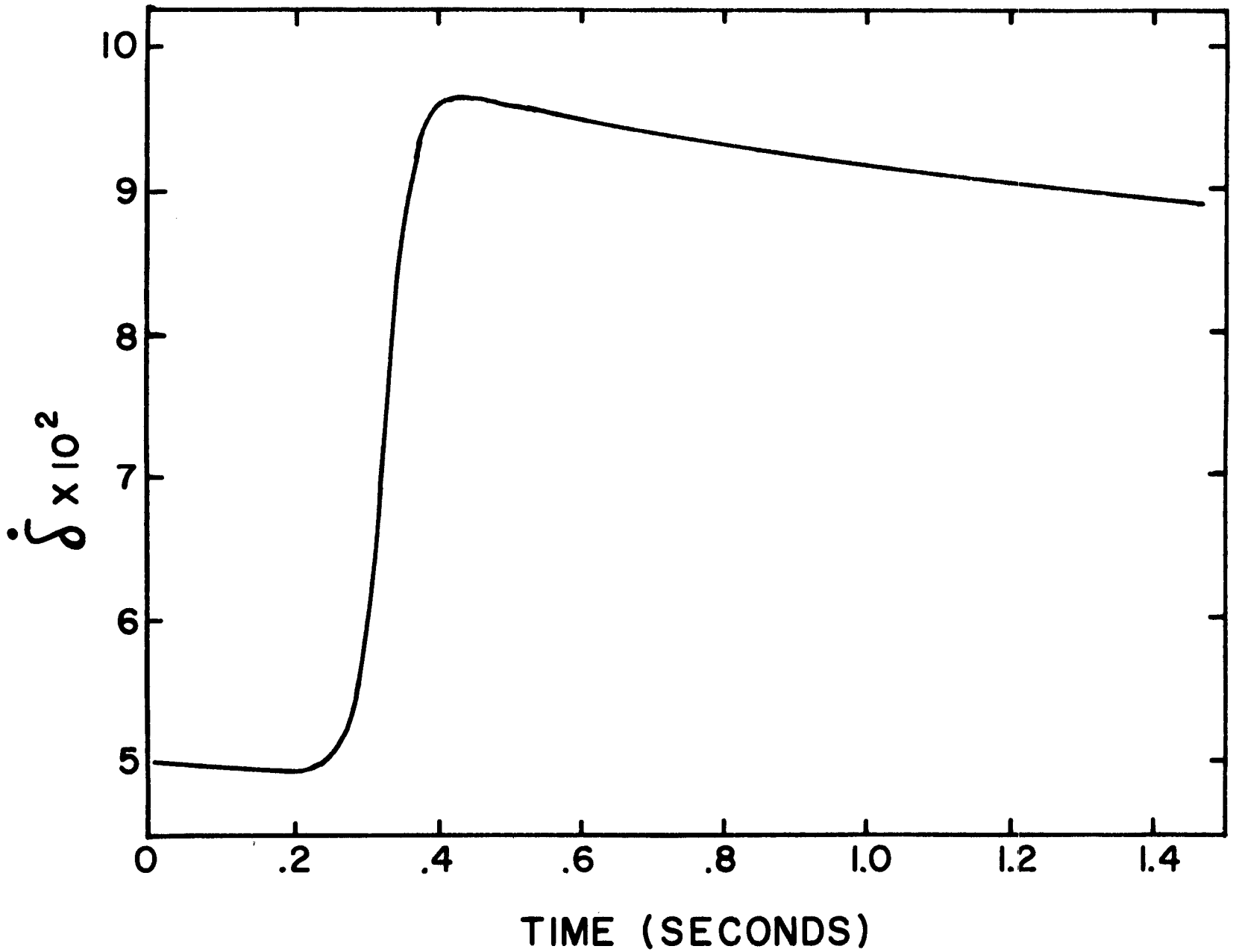
10
9
8
7
6
5
$\dot{\delta} \times 10^2$
0
.2
.4
.6
.8
1.0
1.2
1.4
TIME (SECONDS)

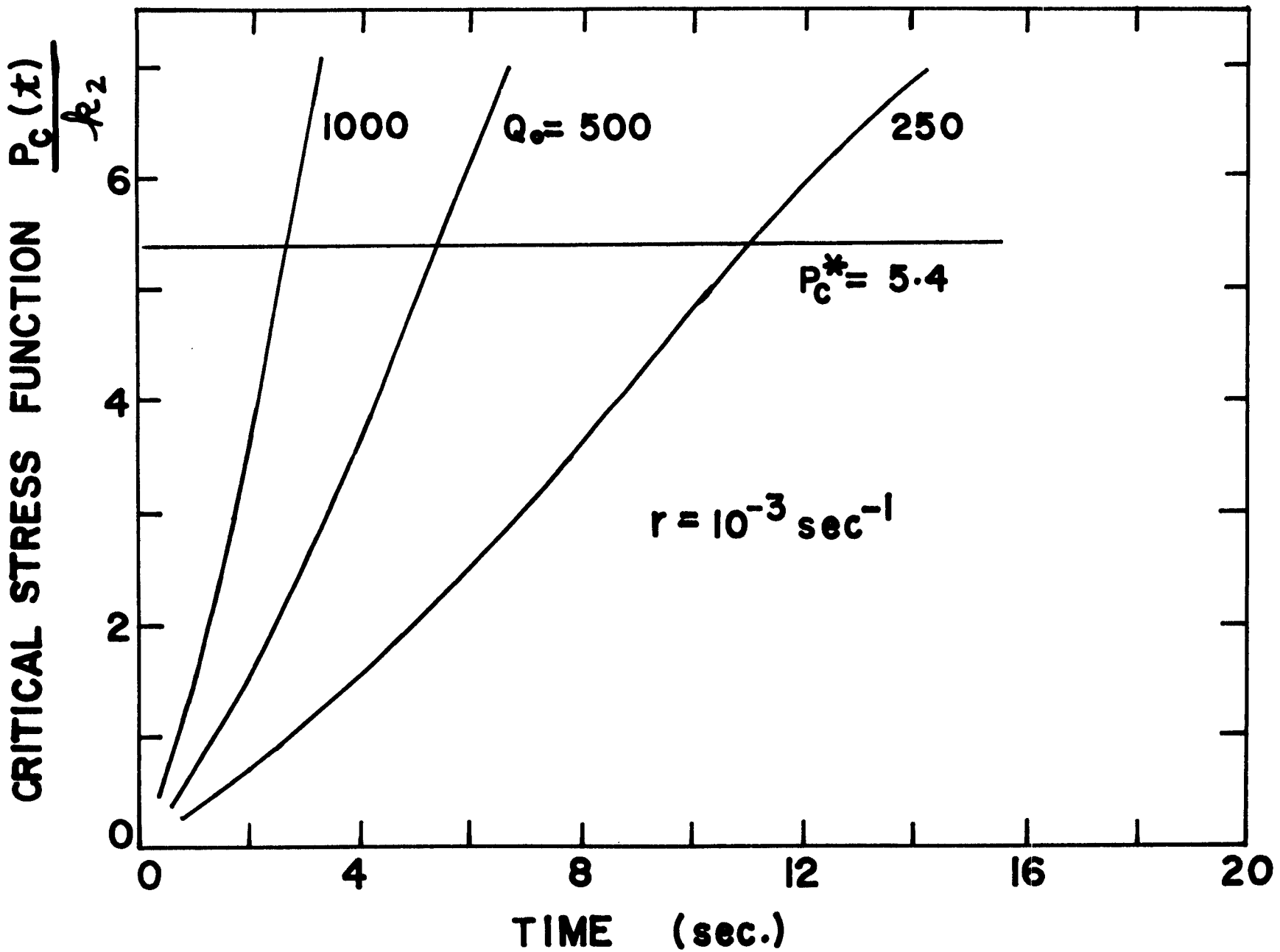
CRITICAL STRESS FUNCTION $\frac{P_c(t)}{k_2}$
1000
Q_e= 500
250
P_c^*= 5.4
r = 10^{-3} sec^{-1}
0
2
4
6
0
4
8
12
16
20
TIME (sec.)

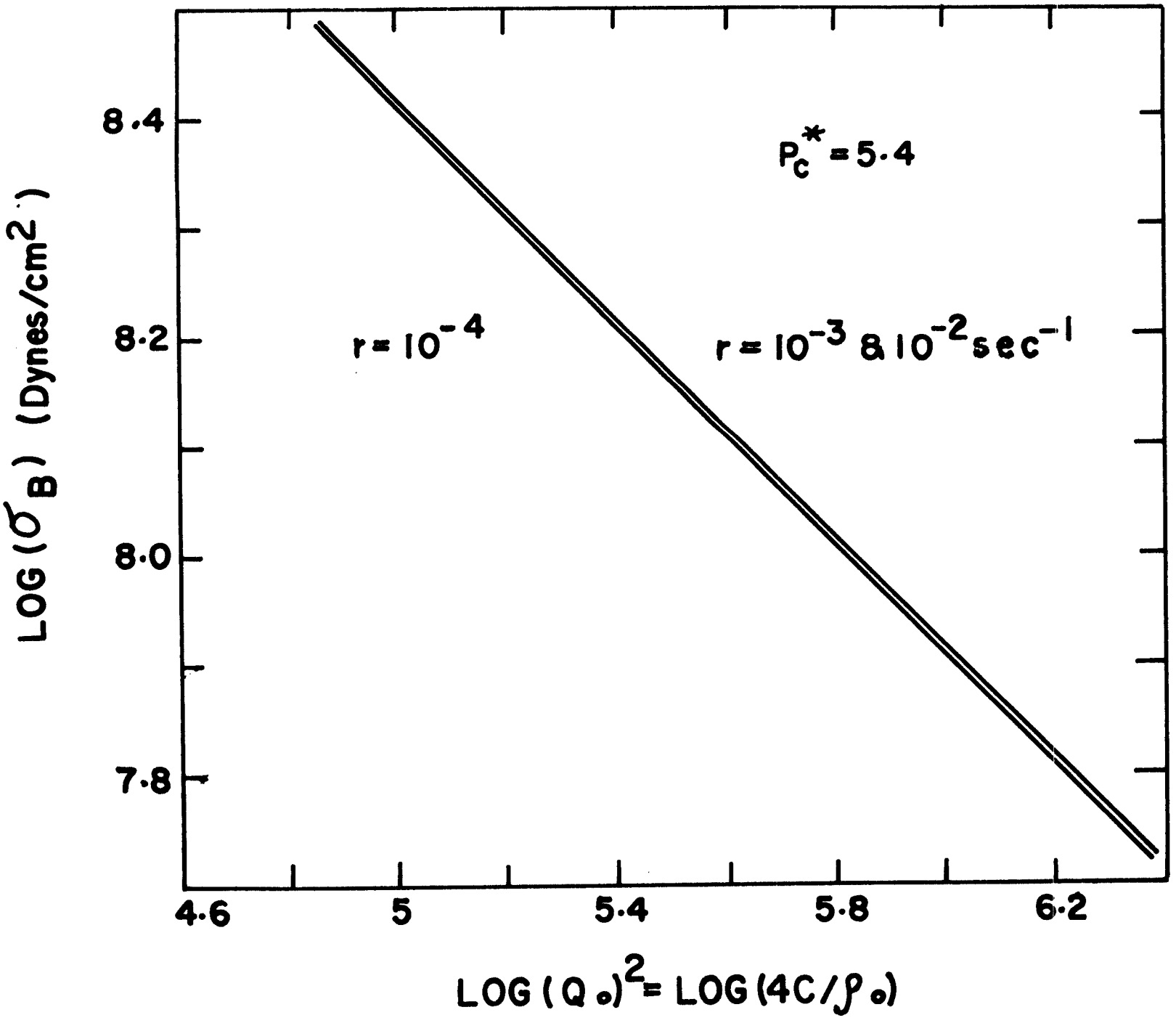
8.4
8.2
8.0
7.8
LOG (σ_B) (Dynes/cm^2)
$P_c^* = 5.4$
$r = 10^{-4}$
$r = 10^{-3}$ & 10^{-2} sec^{-1}
4.6
5
5.4
5.8
6.2
LOG $(Q_o)^2$ = LOG $(4C/\rho_o)$

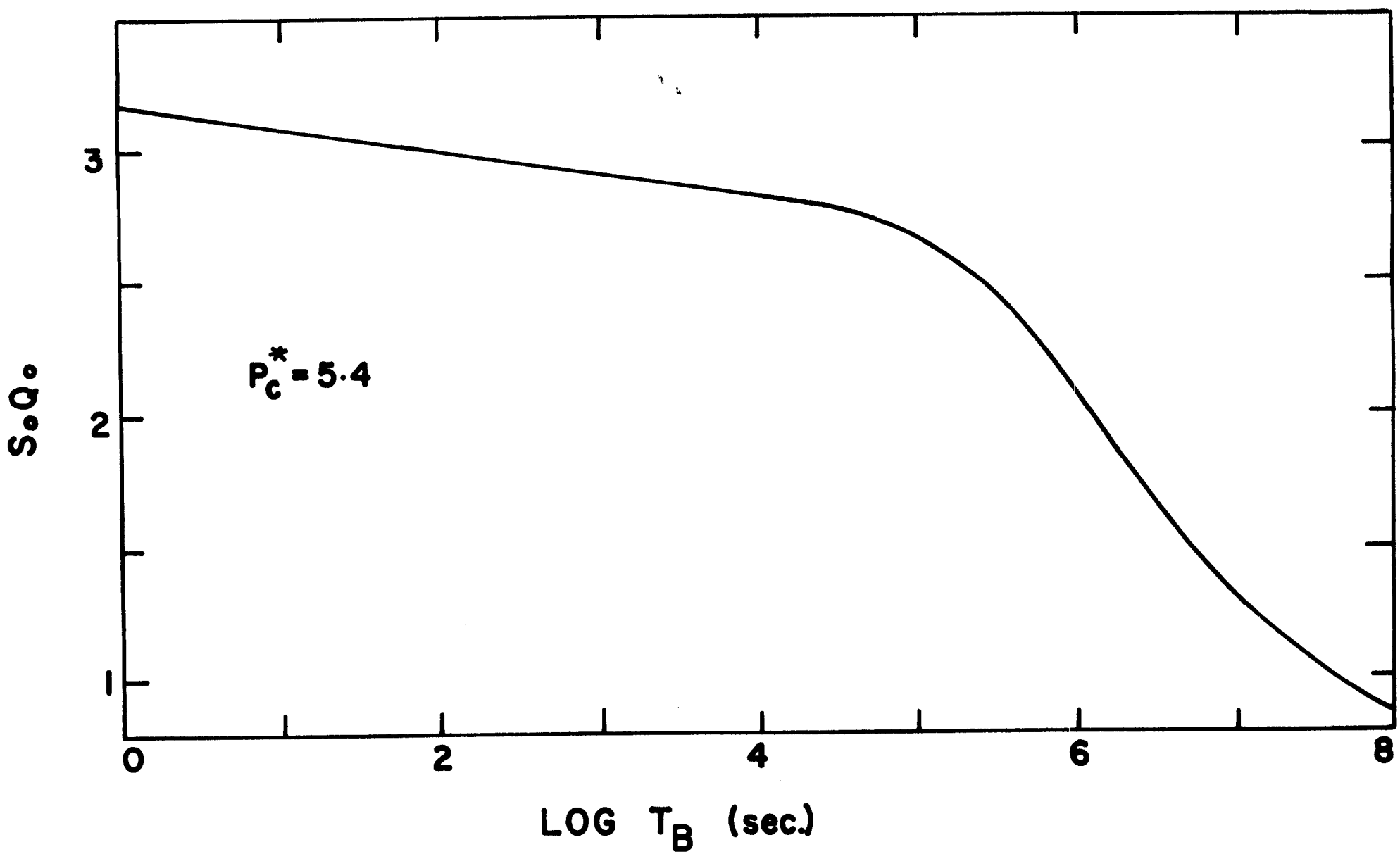
$P_c^* = 5.4$
$S_o Q_o$
3
2
1
0
2
4
6
8
LOG T_B (sec.)

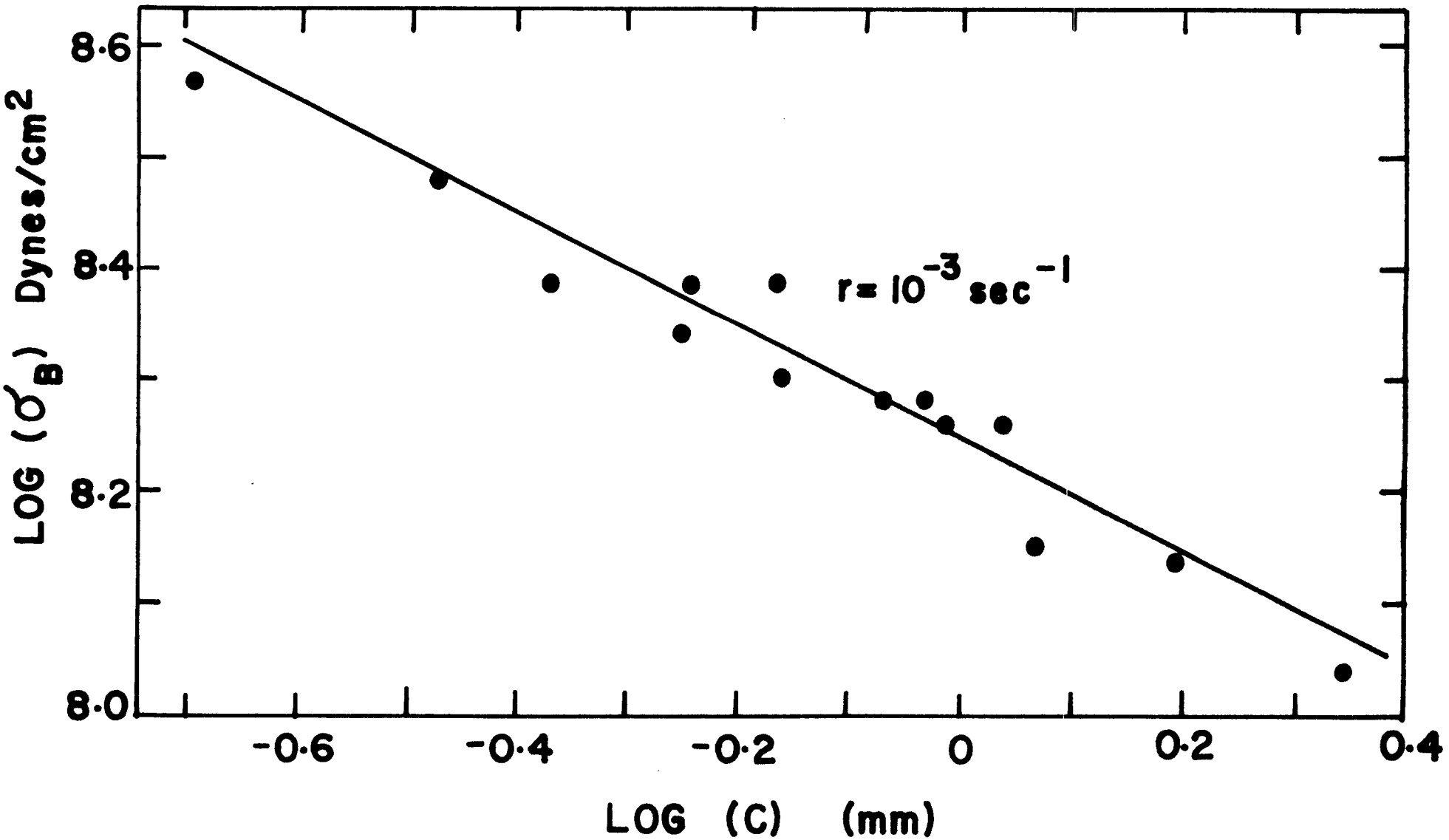
8·6
8·4
8·2
8·0
LOG (σ'_B) Dynes/cm^2
$r = 10^{-3}$ sec^{-1}
-0·6
-0·4
-0·2
0
0·2
0·4
LOG (C) (mm)

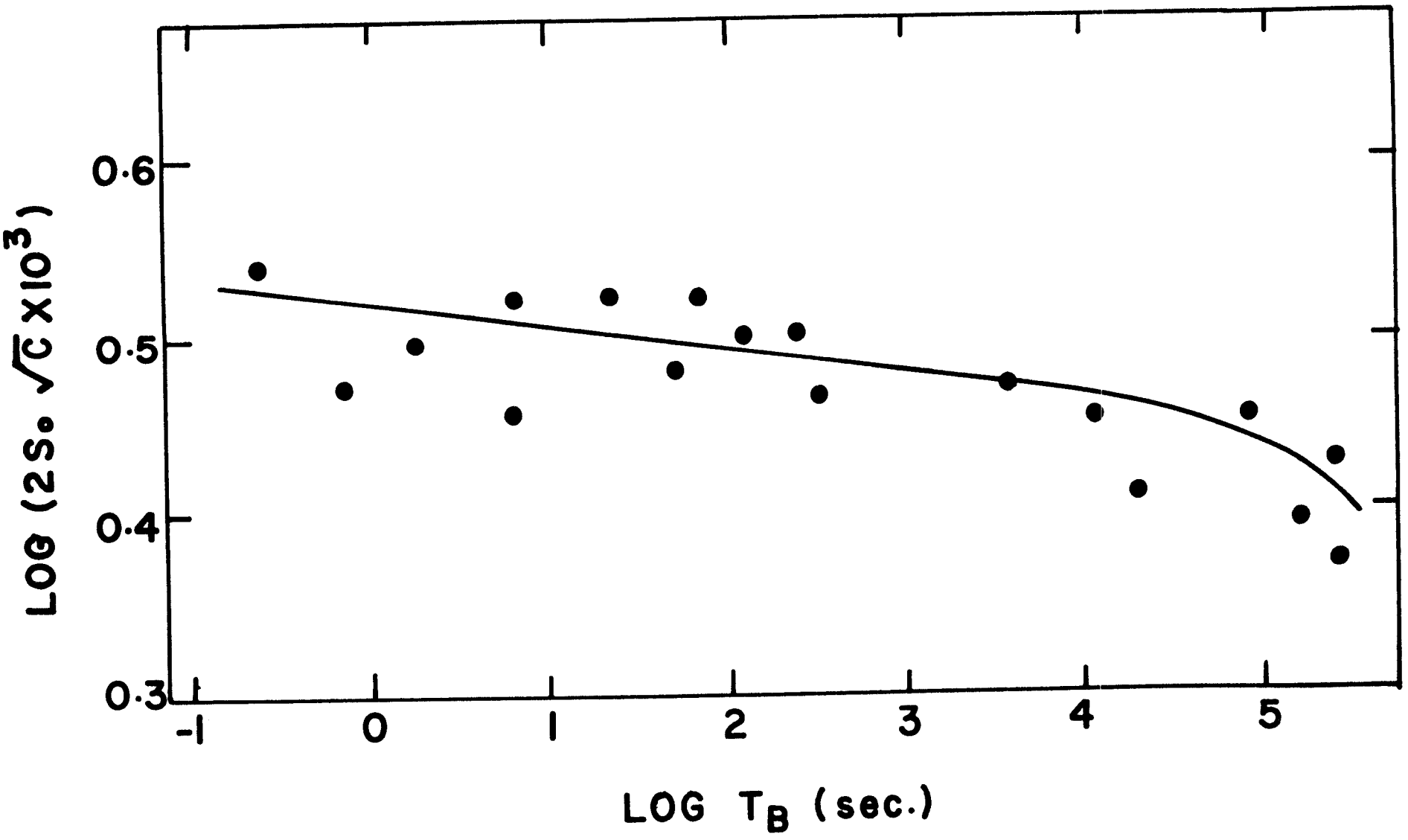
0.6
0.5
0.4
0.3
LOG (2S₀ √C X10³)
-1
0
1
2
3
4
5
LOG T_B (sec.)